A&A 431, 433–449 (2005)
DOI: 10.1051/0004-6361:20041782

Astronomy & Astrophysics

An ISOCAM survey through gravitationally lensing galaxy clusters⋆

IV. Luminous infrared galaxies in Cl 0024+1654 and the dynamical status of clusters

D. Coia[1], B. McBreen[1], L. Metcalfe[2,3], A. Biviano[4], B. Altieri[2], S. Ott[5], B. Fort[6], J.-P. Kneib[7,8], Y. Mellier[6,9], M.-A. Miville-Deschênes[10], B. O'Halloran[1,11], and C. Sanchez-Fernandez[2]

[1] Department of Experimental Physics, University College, Belfield, Dublin 4, Ireland
e-mail: dcoia@bermuda.ucd.ie
[2] XMM-Newton Science Operations Centre, European Space Agency, Villafranca del Castillo, PO Box 50727, 28080 Madrid, Spain
[3] ISO Data Centre, European Space Agency, Villafranca del Castillo, PO Box 50727, 28080 Madrid, Spain
[4] INAF/Osservatorio Astronomico di Trieste, via G.B. Tiepolo 11, 34131, Trieste, Italy
[5] Science Operations and Data Systems Division of ESA, ESTEC, Keplerlaan 1, 2200 AG Noordwijk, The Netherlands
[6] Institut d'Astrophysique de Paris, 98 bis boulevard Arago, 75014 Paris, France
[7] Observatoire Midi-Pyrénées, 14 avenue Edouard Belin, 31400 Toulouse, France
[8] California Institute of Technology, Pasadena, CA 91125, USA
[9] Observatoire de Paris, 61 avenue de l'Observatoire, 75014 Paris, France
[10] Canadian Institute for Theoretical Astrophysics, 60 St-George Street, Toronto, Ontario M5S 3H8, Canada
[11] Dunsink Observatory, Castleknock, Dublin 15, Ireland

Received 3 August 2004 / Accepted 26 October 2004

Abstract. Observations of the core of the massive cluster Cl 0024+1654, at a redshift $z \sim 0.39$, were obtained with the Infrared Space Observatory using ISOCAM at 6.7 μm (hereafter 7 μm) and 14.3 μm (hereafter 15 μm). Thirty five sources were detected at 15 μm and thirteen of them are spectroscopically identified with cluster galaxies. The remaining sources consist of four stars, one quasar, one foreground galaxy, three background galaxies and thirteen sources with unknown redshift. The sources with unknown redshift are all likely to be background sources that are gravitationally lensed by the cluster.

The spectral energy distributions (SEDs) of twelve cluster galaxies were fit from a selection of 20 models using the program GRASIL. The ISOCAM sources have best-fit SEDs typical of spiral or starburst models observed 1 Gyr after the main starburst event. The star formation rates were obtained for cluster members. The median infrared luminosity of the twelve cluster galaxies is $\sim 1.0 \times 10^{11}\ L_{\odot}$, with 10 having infrared luminosity above $9 \times 10^{10}\ L_{\odot}$, and so lying near or above the $1 \times 10^{11}\ L_{\odot}$ threshold for identification as a luminous infrared galaxy (LIRG). The [O II] star formation rates obtained for 3 cluster galaxies are one to two orders of magnitude lower than the infrared values, implying that most of the star formation is missed in the optical because it is enshrouded by dust in the starburst galaxy.

The cluster galaxies in general are spatially more concentrated than those detected at 15 μm. However the velocity distributions of the two categories are comparable. The colour−magnitude diagramme is given for the galaxies within the ISOCAM map. Only 20% of the galaxies that are significantly bluer than the cluster main sequence were detected at 15 μm, to the limiting sensitivity recorded. The counterparts of about half of the 15 μm cluster sources are blue, luminous, star-forming systems and the type of galaxy that is usually associated with the Butcher-Oemler effect. HST images of these galaxies reveal a disturbed morphology with a tendency for an absence of nearby companions. Surprisingly the counterparts of the remaining 15 μm cluster galaxies lie on the main sequence of the colour–magnitude diagramme. However in HST images they all have nearby companions and appear to be involved in interactions and mergers. Dust obscuration may be a major cause of the 15 μm sources appearing on the cluster main sequence. The majority of the ISOCAM sources in the Butcher-Oemler region of the colour–magnitude diagram are best fit by spiral-type SEDs whereas post-starburst models are preferred on the main sequence, with the starburst event probably triggered by interaction with one or more galaxies.

⋆ Based on observations with ISO, an ESA project with instruments funded by ESA Member States (especially the PI countries: France, Germany, The Netherlands and the United Kingdom) and with the participation of ISAS and NASA. This work has also benefitted from ESO program ID 65.O-0489(A).

Finally, the mid-infrared results on Cl 0024+1654 are compared with four other clusters observed with ISOCAM. Scaling the LIRG count in Cl 0024+1654 to the clusters Abell 370, Abell 1689, Abell 2218 and Abell 2390 with reference to their virial radii, masses, distances, and the sky area scanned in each case, we compared the number of LIRGs observed in each cluster. The number in Abell 370 is smaller than expected by about an order of magnitude, even though the two clusters are very similar in mass, redshift and optical richness. The number of LIRGs detected in each of Abell 1689, Abell 2218 and Abell 2390 is 0, whereas 3 were expected from the comparison with Cl 0024+1654. A comparison of the mid-infrared sources in Abell 1689 and Abell 2218 shows that the sources in Abell 1689 are more luminous and follow the same trend identified in the comparison between Cl 0024+1654 and Abell 370. These trends seem to be related to the dynamical status and history of the clusters.

Key words. galaxies: clusters: general – galaxies: clusters: individual: Cl 0024+1654 – infrared: galaxies

1. Introduction

Clusters of galaxies contain thousands of members within a region a few Mpc in diameter, and are the largest known gravitationally bound systems of galaxies, having masses up to 10^{15} $M_\odot$ for the richest systems. In hierarchical models clusters of galaxies grow by accreting less massive groups falling along filaments at a rate governed by the initial density fluctuation spectrum, the cosmological parameters and the nature and amount of dark matter. In the cluster environment, newly added galaxies are transformed from blue, active star forming systems, to red, passive ellipticals, undergoing a morphological evolution stronger than that of field galaxies at a similar redshift (Gavazzi & Jaffe 1987; Byrd & Valtonen 1990; Abraham et al. 1996b). The cluster galaxy population is also characterized by a lower star formation rate (SFR) than field galaxies of similar physical size and redshift (Couch et al. 2001; Lewis et al. 2002).

Butcher & Oemler (1978) showed that clusters of galaxies generally have a fraction f_B of blue galaxies[1] that increases with cluster redshift, ranging from a value near 0 at $z = 0$, to 20% at $z = 0.4$ and to 80% at $z = 0.9$, suggesting a strong evolution in clusters (Rakos & Schombert 1995). The galaxies responsible for the Butcher-Oemler effect (hereafter BO effect) are generally luminous, spirals, and emission-line systems, with disturbed morphologies. The high resolution imaging achieved by the Hubble Space Telescope (HST) has greatly improved morphological studies of the cluster galaxy population over a wide range in redshift. The mixture of Hubble types in distant clusters is significantly different from that seen in nearby systems. The population of star-forming and post-starburst galaxies are disk dominated systems, some of which are involved in interactions and mergers. (Abraham et al 1996a; Stanford et al. 1998; Couch et al. 1998; Van Dokkum et al. 1998; Morris et al. 1998; Poggianti et al. 1999; Best 2000).

Many mechanisms have been proposed to explain the complicated processes that occur in clusters, including ram pressure stripping of gas (Gunn & Gott 1972), galaxy harassment (Moore et al. 1996; Moss & Whittle 1997), galaxy infall (Ellingson et al. 2001), cluster tidal forces (Byrd & Valtonen 1990; Fujita 1998) and interactions with other cluster galaxies (Icke 1985; Moss & Whittle 1997). The main processes responsible for the morphological and spectral evolution of cluster galaxies have yet to be determined. Ram pressure and tidal effects can quench the star formation activity gradually because they operate over a period longer than 1 Gyr (e.g. Ghigna et al. 1998; Ramirez & de Souza 1998). Galaxy-galaxy interactions, galaxy harassment and cluster mergers can enhance it and produce changes in galaxy properties over timescales of ∼100 Myr (e.g. Lavery & Henry 1986; Moore et al. 1996). Recent changes in the properties of the galaxies may be detectable in the mid-infrared if associated with a burst of star formation.

In the context of our ongoing exploitation of mid-infrared cluster data obtained with ESA's Infrared Space Observatory (ISO, Kessler et al. 1996), we have analysed ISO observations of Abell 370, Abell 2218 and Abell 2390 (Metcalfe et al. 2003; Altieri et al. 1999; Biviano et al. 2004), Abell 2219 (Coia et al. 2005), and Cl 0024+1654 (this paper). In common with other surveys we have found that mid-infrared observations of field galaxies from deep surveys reveal a population of starburst galaxies that evolve significantly with redshift (Aussel et al. 1999; Oliver et al. 2000; Serjeant et al. 2000; Lari et al. 2001; Gruppioni et al. 2002; Elbaz & Cesarsky 2003; Metcalfe et al. 2003; Sato et al. 2003). This class of sources are Luminous and Ultraluminous infrared galaxies (LIRGs and ULIRGs, Sanders & Mirabel 1996; Genzel & Cesarsky 2000), have SFRs of ∼100 $M_\odot\,\mathrm{yr}^{-1}$ (Oliver et al. 2000; Mann et al. 2002) and seem to be almost always the result of galaxy-galaxy interactions at least in the local Universe (Veilleux et al. 2002). The ISOCAM sources account for most of the contribution of the mid-infrared to the Cosmic Infrared Background (CIRB, Altieri et al. 1999; Franceschini et al. 2001; Metcalfe et al. 2001, 2003; Elbaz et al. 2002). Studies of the global SFR show a decline by a factor of 3−10 since the peak of star formation at $z = 1$−2 (Madau et al. 1996; Steidel et al. 1999; Elbaz & Cesarsky 2003). The downturn in the global SFR and population of LIRGs and ULIRGs may be caused by galaxies running out of gas available for star formation and the buildup of large scale structure in the Universe that changed the environment of galaxies.

A study of the impact of the environment on galaxies in clusters could help in understanding the global SFR. Mid-infrared observations have been published for local clusters (Boselli et al. 1997, 1998; Contursi et al. 2001) and distant clusters of galaxies (Pierre et al. 1996; Lémonon et al. 1998; Altieri et al. 1999; Fadda et al. 2000; Metcalfe et al. 2003; Coia et al. 2005). In Abell 2390, Abell 370 and Abell 2218 the greater part of the 15 μm sources for which spectroscopic redshifts are available are found to be background sources (Metcalfe et al. 2003). However Fadda et al. (2000) and Duc et al. (2002)

[1] Blue galaxies are defined as brighter than $M_V = -19.26$ (with $H_0 = 70\,\mathrm{km\,s^{-1}\,Mpc^{-1}}$) with rest-frame $B-V$ colours at least 0.2 magnitudes bluer than those of the E/S0 galaxy sequence at the same absolute magnitude (Butcher & Oemler 1984; Oemler et al. 1997).

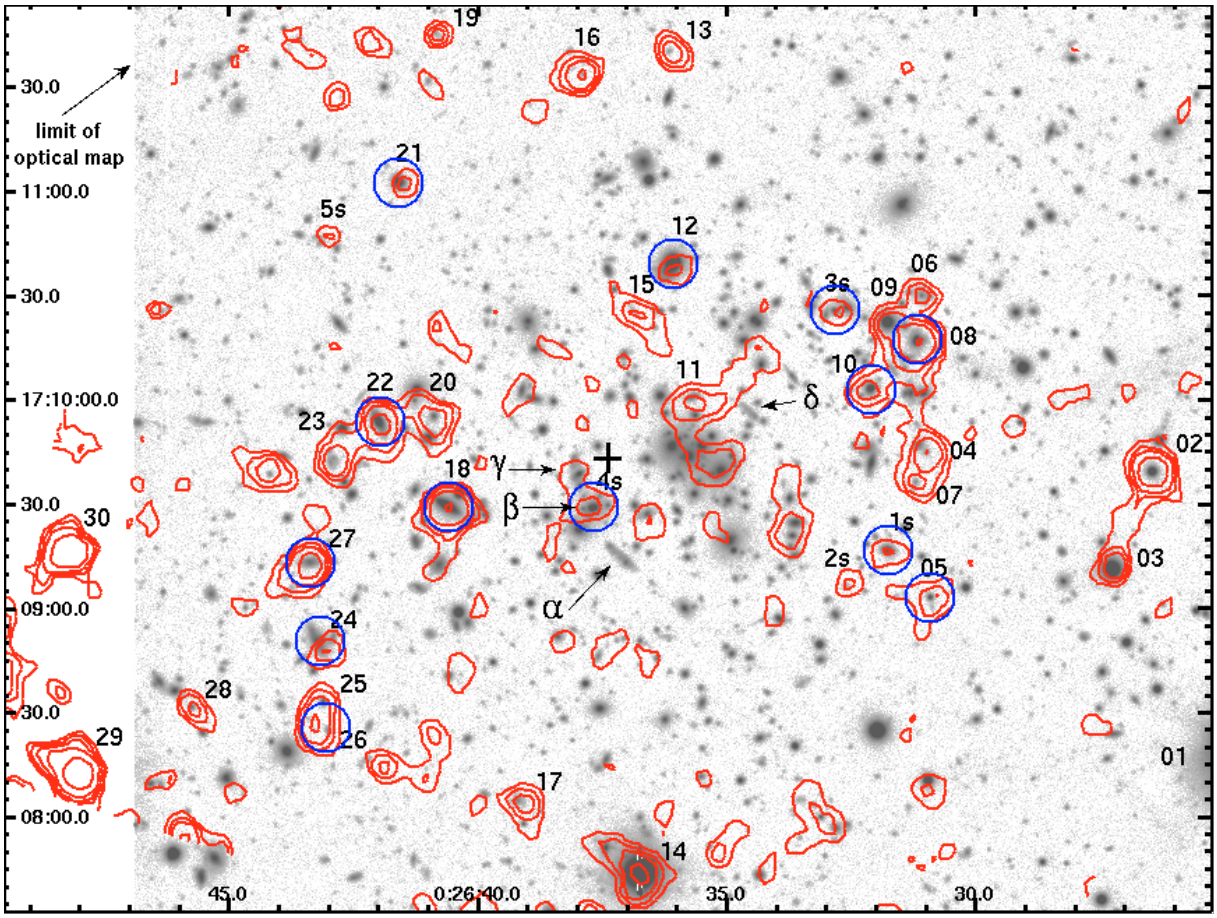

Fig. 1. The 15 μm contour map (red) of Cl 0024+1654 overlaid on a Very Large Telescope image taken in the V band with the FORS2 instrument (ESO program identification: 65.O-0489(A)). Numbers 1 to 30 refer to the 15 μm sources in the primary list (Table 2) and sources 1s to 5s label sources from the supplementary list (Table 3). Each set of sources is labelled in order of increasing Right Ascension. Sources ISO_Cl0024_29 and ISO_Cl0024_30 are outside the boundary of the optical map, and have a star and a faint galaxy, respectively, as optical counterparts. Blue circles denote 15 μm sources that are spectroscopically confirmed cluster galaxies. Greek letters ($\alpha \div \delta$) identify four gravitationally lensed images of the background galaxy associated with the spectacular giant arcs in the cluster field. North is up and East is to the left. The centre of the ISO map, indicated by a cross, is at RA 00 26 37.5 and Dec 17 09 43.4 (J2000).

found a higher proportion of 15 μm cluster sources in the cluster Abell 1689 at $z = 0.18$ and Duc et al. (2004) discovered many LIRGs in the cluster J1888.16CL at $z = 0.56$.

In this work we focus on the mid-infrared properties of the galaxy cluster Cl 0024+1654. The paper is organized as follows: Sect. 2 contains a description of the cluster. Section 3 describes the infrared observations and outlines the data reduction, source extraction and calibration processes. Section 4 presents the results, the model spectral energy distributions (SEDs) and star formation rates for cluster galaxies. Section 5 describes the spatial, redshift and colour properties of cluster galaxies and contains a description of Hubble Space Telescope images of some galaxies detected by ISOCAM. Section 6 makes a comparison between Cl 0024+1654 and other clusters studied, including Abell 1689, Abell 370, Abell 2390 and Abell 2218. The conclusions are in Sect. 7. The Appendix contains additional comments on some of the ISOCAM sources.

We adopt $H_0 = 70\,\mathrm{km\,s^{-1}\,Mpc^{-1}}$, $\Omega_\Lambda = 0.7$ and $\Omega_\mathrm{m} = 0.3$. With this cosmology, the luminosity distance to the cluster is $D_L = 2140$ Mpc and $1''$ corresponds to 5.3 kpc at the cluster redshift. The age of the Universe at the cluster redshift of 0.39 is 9.3 Gyr.

2. The cluster

Cl 0024+1654 is a rich cluster of galaxies at redshift $z \sim 0.395$ (Humason & Sandage 1957; Gunn & Oke 1975; Smail et al. 1993). It has a spectacular system of gravitationally lensed arcs (Fig. 1) that were first observed by Koo (1988) and subsequently studied by Mellier et al. (1991), Kassiola et al. (1994), Wallington et al. (1995) and Smail et al. (1997). The main arc is split into segments (Colley et al. 1996; Tyson et al. 1998) and is the lensed image of a background blue galaxy at redshift $z = 1.675$ (Broadhurst et al. 2000). Unlike other clusters of galaxies, such as Abell 2218 or Abell 2390 that have arc-like features, Cl 0024+1654 does not have a central dominant cD galaxy.

Cl 0024+1654 was one of the two clusters examined by Butcher & Oemler (1978) in their first published work on galaxy colours. The fraction of blue galaxies in Cl 0024+1654 is $f_B = 0.16$ which is much larger than the values of $f_B = 0.04$

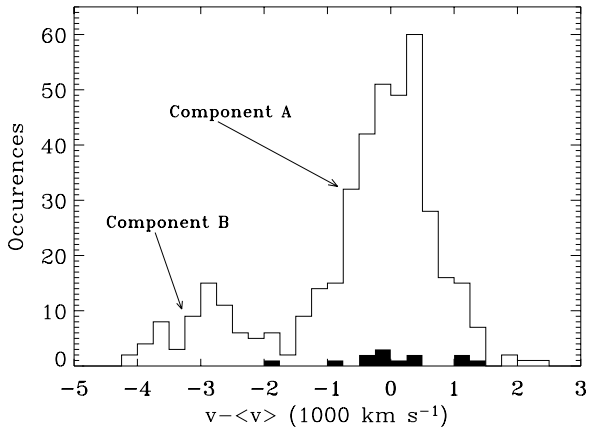

Fig. 2. The fractional distribution of velocities of cluster galaxies in Cl 0024+1654. The counterparts of the cluster members detected at 15 μm are displayed in bold. All velocities are in the cluster rest-frame.

and $f_B = 0.03$ for the Virgo ($z = 0.003$) and Coma ($z = 0.02$) clusters respectively (Butcher & Oemler 1984; Dressler et al. 1985; Schneider et al. 1986).

The determination of the spectral types of galaxies has been made for the cluster and the field (Czoske et al. 2002; Balogh et al. 2002). Using a wide field HST survey of Cl 0024+1654, Treu et al. (2003) found that the fraction of early-type galaxies (E+S0) is highest (∼73%) in the cluster core, declines rapidly to about 50% at ∼1 Mpc, and reaches the background value of ∼43% at the periphery of the cluster (at a radius of ∼5 Mpc).

The mass profile of the cluster has been inferred from gravitational lensing analyses, kinematical analyses of the redshifts of the cluster galaxies, and X-ray observations. The low value of the X-ray luminosity implies a mass 2 to 3 times smaller than that predicted by lensing models (Soucail et al. 2000; Ota et al. 2004). There are also differences among the lensing models. Broadhurst et al. (2000) favour a cuspy NFW (Navarro et al. 1997) profile for the mass distribution of the cluster. Tyson et al. (1998) argue that this result requires an average cluster velocity distribution much higher than the measured value of $\sigma_v \sim 1150\,\mathrm{km\,s^{-1}}$ (Dressler et al. 1999) and favour a uniform-density core for the halo mass profile. The weak lensing analysis made by Kneib et al. (2003), based on an extensive HST survey of Cl 0024+1654 (Treu et al. 2003), indicates that the region within 5 Mpc from the centre of the cluster is well fit by a steep NFW-like profile, and the isothermal fit is strongly rejected. Ota et al. (2004) analysed the X-ray emission from the cluster and found that an isothermal model with a mean temperature of 4.4 keV is a good fit to the temperature distribution. They also estimated the mass of the cluster on the assumption that the intracluster medium is in hydrostatic equilibrium, and confirmed that the mass inferred from X-ray observations is smaller than the mass predicted by lensing models by a factor of about 3. The complex structure of the central region of the cluster might explain the discrepancy (Zhang et al. 2005).

During an extensive spectroscopic survey of Cl 0024+1654, Czoske et al. (2001) detected a significant number of galaxies at a redshift slightly lower than that of the cluster (Fig. 2). This concentration (component B) is interpreted as a small, less massive cluster superimposed on the main cluster (component A) and lying at a mean redshift of $z = 0.381$. Numerical simulations indicate that the two clusters in Cl 0024+1654 are involved in a high-speed collision along the line-of-sight to the cluster (Czoske et al. 2002). The relative velocity of the two components, derived from the difference in redshift of the two main galaxy concentrations, is about 3000 $\mathrm{km\,s^{-1}}$. The collision scenario is not unusual because 30–40% of galaxy clusters have substructures that are detected in optical, X-ray and radio observations (e.g. Dressler & Shectman 1988; Schuecker et al. 2001; Mercurio et al. 2003). These substructures indicate that the hosting clusters are not fully dynamically relaxed and might be currently undergoing, or have recently undergone, mergers. The important results obtained by Czoske et al. (2001, 2002) may give a new insight into the BO effect in medium and high redshift clusters. The impact of the two clusters could have triggered star formation in cluster galaxies, especially those on the leading edge of the smaller cluster, thus generating the large number of blue galaxies observed in Cl 0024+1654. The differences between the results from the methods used to determine the mass of Cl 0024+1654 are naturally explained by the cluster collision (Czoske et al. 2002).

3. Observations, data reduction and source detection

3.1. Observations

The core of the cluster Cl 0024+1654 was observed at 7 μm and 15 μm using the *LW*2 and *LW*3 filters of the camera ISOCAM (Cesarsky et al. 1996) on board ISO. The ISOCAM long wavelength (*LW*) detector consisted of a 32×32 SiGa array. The observations were made on June 9 and June 15, 1997, in raster mode, with an on-chip integration time of 5.04 s in the 3″ per pixel field of view, and cover an area of approximately 38 square arcminutes. A discussion of the relevant observing strategy for ISOCAM can be found in Metcalfe et al. (2003) (with the exception that the Cl 0024+1654 rasters were not "micro-scanned" with sub-pixel finesse. I.e. the raster step sizes were multiples of the array pixel size, whereas Metcalfe et al. describe rasters with step sizes involving fractions of a pixel's dimensions). For each pointing of the raster, 14 readouts were performed at 7 μm and 10 at 15 μm. Fifty readouts were taken at the beginning of each raster to allow for detector stabilization. The parameters used for the observations are given in Table 1, which also lists the 5σ sensitivity reached after data processing. The diameter of the point spread function (PSF) central maximum at the first Airy minimum is $0.84\times\lambda(\mu\mathrm{m})$ arcseconds. The *FWHM* is about half that amount and Okumura (1998) obtained values of 3.3″ at 7 μm and 5″ at 15 μm for the PSF *FWHM* in the 3″ per pixel field-of-view. The data were reduced and, to take advantage of a slight deliberate offset between the two 15 μm maps, were rebinned so that the final map has a pixel size of 1″, with potential for slightly improved spatial resolution. The maximum depth is reached toward the centre of the rasters, where the dwell time per position on the sky is greatest. As recorded in Table 1, two rasters were made at

Table 1. Observational parameters used. The observations were made with the ISOCAM *LW*2 (5–8.5 μm) and *LW*3 (12–18 μm) filters at their respective reference wavelengths of 6.7 μm and 14.3 μm. On-chip integration time was always 5.04 seconds and the 3″ per-pixel-field-of-view was used. *M* and *N* are the number of steps along each dimension of the raster, while dm and dn are the increments for a raster step. The sensitivity in μJy is given at the 5σ level. The table also includes the total area covered and the number of readouts per raster step. The rasters were repeated *k* times. Tot. t is the total time dedicated to each filter observation.

Filter	$\lambda_{\rm ref}$ (μm)	*n* Steps *M*	*N*	d*m* (″)	d*n* (″)	Reads per step	area ($'^2$)	Done *k* times	Sensitivity (μJy)	Tot. *t* (sec)
*LW*2	6.7	6	6	45	45	14	28.6	1	400	3138
*LW*3	14.3	14	14	21	21	10	37.8	2	140	22 615

15 μm and a single raster at 7 μm that had a larger step size and less observation time (by a factor of 7).

3.2. Data reduction

The data were reduced using the *ISO***C***AM* **I***nteractive* **A***nalysis* System or CIA (Delaney & Ott 2002; Ott et al. 1997) in conjunction with dedicated routines, following the method[2] described in Metcalfe et al. (2003). The two 15 μm raster maps were normalized to their respective redundancy maps[3] and merged into a single raster, thus increasing the sensitivity of the map to faint sources.

The 15 μm sources were found by visually inspecting the merged and the two individual maps. Detections common to the three maps are given in the *primary source list* (Table 2). The selection criterion adopted is very conservative because it requires the source to be detected in both individual rasters, resulting in the rejection of faint sources that can be detected only in the merged map. Therefore we include a *supplementary list* containing sources found in the merged map and in at least one of the individual rasters (Table 3). The fluxes of the sources were computed by aperture photometry using a circular aperture of 9″ diameter, centred on the infrared source.

Since there was only one raster at 7 μm, an independent comparison of source detections was not possible and real sources were considered to be only those having a 15 μm counterpart.

The optical data were obtained on the ESO/VLT during October 2001 with the VLT/FORS instrument in service mode[4]. The data have been processed at the TERAPIX data center[5]. Pre-calibrations, astrometric and photometric calibrations as well as image stacking and catalog production were done using standard CCD image processing algorithms and tools available at the TERAPIX center (see McCracken et al. 2003 for details).

3.3. Monte Carlo simulations and calibration

Monte Carlo simulations were performed to calibrate the complex data reduction process by characterizing how it affects model point sources with known properties inserted into the raw data, and to characterize the precision with which source signals could be recovered from the data. The procedure adopted is fully described in Metcalfe et al. (2003), the only exception being that all photometry performed for the present work employed the XPHOT routine in CIA, whereas Metcalfe et al. used SExtractor (Bertin & Arnouts 1996). The fluxes of the inserted fake sources were measured in exactly the same way as the fluxes of the real sources. The simulations were performed independently for all rasters. The fluxes of the inserted fake sources were measured by manual photometry adopting the same parameters, i.e. same aperture, used for the real sources. The simulations establish the relationship between source signal detected in the photometric aperture, and total source signal actually collected in the detector. Signal in the photometric aperture can therefore be scaled to total signal, but at this point the units are detector units, or ADUgs. The relationship between source signal deposited in the detector and actual source flux-density in mJy is determined by two further scaling factors. (a) A filter specific ISOCAM calibration factor relating stabilised source signal, in detector units, to mJy, i.e. 1 ADU per gain per second (ADUgs) $\equiv$ 0.43 mJy for *LW*2 and 1 ADUgs $\equiv$ 0.51 mJy for *LW*3 (Delaney & Ott 2002); and (b) a correction for detector responsive transient effects which cause the signal from faint sources to fall below that expected on the basis of bright reference source measurements. The derivation of that scaling factor, in the context of the reduction algorithm applied here, is described in Metcalfe et al. (2003) and references therein.

4. Results

The merged 15 μm map (Fig. 1) is overlaid on a *V*-band image of the cluster taken with the Very Large Telescope (VLT).

[2] An interesting alternative approach, optimised for extended-source detection, but which gives very good overall results and can be used to cross-check the validity of the faintest detections, is the method of Miville-Deschênes et al. (2000). We employed products of this alternative reduction process (SLICE) as a further cross-check of the reality of the faintest sources in our lists, reasoning that both methods would tend to preserve real sources, while any residual glitches affecting the results of our primary analysis would have some probability of being filtered out in the independent SLICE analysis. To arrive at our final list we rejected some very faint candidate sources as being unreliable when they were poorly reproduced by this independent analysis route. We consider this approach to be very conservative.

[3] The "redundancy" of a point in a raster map refers to the number of raster steps for which that point on the sky has been seen by some detector pixel.

[4] Program ID: 65.0-489A FORS; PI: Fort.

[5] `http://terapix.iap.fr`

Table 2. The primary list of sources detected at 15 μm. The columns are (from left to right): source identification number in order of increasing Right Ascension; source flux and precision before calibration (in ADUgs); source flux and precision after calibration (in mJy); Right Ascension and Declination of the infrared source (J2000); redshift and name of the optical counterpart, if known. The redshift of source ISO_Cl0024_02 was taken from Schmidt et al. (1986). All other redshifts are from Czoske et al. (2001) or provided by T. Treu (private communication). The names of the stars are from HEASARC.

Source ID ISO_Cl0024	Signal (ADU)	Precision (±ADU)	Flux (mJy)	Precision (±mJy)	RA (J2000)	Dec (J2000)	z if known	Name of optical counterpart if known
01	0.634	0.090	0.786	0.120	00 26 24.3	+17 08 18.0	Star	TYC 1180-82-1
02	0.472	0.060	0.577	0.090	00 26 26.3	+17 09 39.0	0.959	PC 0023+1653
03	0.256	0.060	0.298	0.080	00 26 27.0	+17 09 11.7	Star	N3231320329
04	0.298	0.060	0.352	0.080	00 26 30.8	+17 09 44.8	–	
05	0.184	0.060	0.205	0.080	00 26 30.7	+17 09 03.5	0.3935	
06	0.230	0.060	0.264	0.080	00 26 30.9	+17 10 29.4	–	
07	0.217	0.060	0.247	0.080	00 26 31.0	+17 09 37.4	–	
08	0.610	0.090	0.755	0.120	00 26 31.0	+17 10 15.6	0.4005	
09	0.286	0.060	0.336	0.080	00 26 31.5	+17 10 21.4	0.2132	
10	0.191	0.060	0.214	0.080	00 26 31.8	+17 10 03.5	0.4000	
11	0.220	0.060	0.251	0.080	00 26 35.5	+17 09 59.1	0.5558	
12	0.182	0.060	0.202	0.080	00 26 35.9	+17 10 36.4	0.3860	
13	0.210	0.060	0.238	0.080	00 26 35.9	+17 11 39.9	–	
14	0.293	0.060	0.346	0.080	00 26 36.6	+17 07 44.4	Star	EO903-0219757
15	0.170	0.060	0.186	0.080	00 26 36.6	+17 10 25.4	–	
16	0.260	0.060	0.302	0.080	00 26 37.7	+17 11 33.4	–	
17	0.253	0.060	0.293	0.080	00 26 38.9	+17 08 03.9	–	
18	0.634	0.090	0.786	0.120	00 26 40.4	+17 09 28.7	0.394	
19	0.187	0.060	0.208	0.080	00 26 40.6	+17 11 44.9	–	
20	0.262	0.060	0.305	0.080	00 26 40.7	+17 09 54.0	0.7125	
21	0.191	0.060	0.213	0.080	00 26 41.3	+17 11 01.4	0.3924	
22	0.334	0.060	0.398	0.080	00 26 41.8	+17 09 52.9	0.3935	
23	0.282	0.060	0.331	0.080	00 26 42.7	+17 09 41.6	–	
24	0.189	0.060	0.211	0.080	00 26 42.8	+17 08 48.5	0.3954	
25	0.200	0.060	0.225	0.080	00 26 42.9	+17 08 31.7	0.9174	
26	0.324	0.060	0.385	0.080	00 26 43.1	+17 08 25.1	0.3961	
27	0.373	0.060	0.449	0.080	00 26 43.2	+17 09 11.7	0.3932	
28	0.120	0.060	0.122	0.080	00 26 45.5	+17 08 30.8	–	
29	0.946	0.110	1.191	0.140	00 26 47.9	+17 08 12.0	Star	EO903-0219375
30	0.489	0.070	0.598	0.090	00 26 48.0	+17 09 15.7	–	

Table 3. The supplementary list of 15 μm sources. The meaning of the columns is the same as in Table 2.

Source ID ISO_Cl0024	Signal (ADU)	Precision (±ADU)	Flux (mJy)	Precision (±mJy)	RA (J2000)	Dec (J2000)	z if known
1s	0.150	0.060	0.160	0.080	00 26 31.6	+17 09 17.1	0.3998
2s	0.190	0.060	0.212	0.080	00 26 32.4	+17 09 06.5	–
3s	0.124	0.060	0.127	0.080	00 26 32.6	+17 10 26.1	0.3965
4s	0.173	0.060	0.190	0.080	00 26 37.4	+17 09 29.1	0.3900
5s	0.182	0.060	0.202	0.080	00 26 42.9	+17 10 45.6	–

Table 4. The list of 7 μm sources with source flux exceeding 5σ of the local noise, and having 15 μm counterparts. From left to right: 15 μm source identification number as listed in Table 2; signal and precision of flux in ADU; flux and precision in mJy; Right Ascension, Declination; nature of the source; and finally the [7 μm]/[15 μm] colour ratio.

Source ID	Signal (ADU)	Precision (±ADU)	Flux (mJy)	Precision (± mJy)	RA (J2000)	Dec (J2000)	Notes	[7 μm]/[15 μm]
03	1.461	0.219	1.685	0.253	00 26 27.0	+17 09 08.2	Star	5.7
14	1.276	0.191	1.468	0.220	00 26 36.5	+17 07 41.0	Star	4.2
29	3.806	0.571	4.427	0.664	00 26 47.9	+17 08 11.1	Star	3.7

The list of sources detected in the two individual 15 μm maps is given in Table 2 and a supplementary list is given in Table 3 (see Sect. 3). The name of the ISOCAM source is composed of the satellite acronym (ISO), the partial name of the cluster (Cl0024), and an identification number assigned to each source.

The 7 μm fluxes for the stars, and their [7 μm]/[15 μm] flux ratios, are given in Table 4. The labels of the 7 μm sources are taken to be the same as their 15 μm counterparts. The fourth star detected at 15 μm (ISO_Cl0024_01) is outside the boundary of the 7 μm raster. No other sources were detected above the 5σ limit of ~400 μJy.

The column named "Precision" in Tables 2 and 3 reflects the repeatability of the photometric results in the fake source simulations. For each source brightness the precision is the 1σ scatter found in the recovered fluxes of fake sources of similar brightness inserted into the raw data. It should be noted that the ratio signal/precision is not, however, the signal-to-noise ratio; nor is it the significance of a source detection. The precision, as defined here, includes, for example, signal deviations caused by residual glitches around the map and by variations in residual background level across the map, which are of course factors that can influence the accuracy of source photometric measurements. However, the significance of an individual source detection must be determined through an examination of the pixel-to-pixel signal variations in the map local to the source. All of the sources listed in Tables 2 and 3 have significance values greater than 5σ. The quoted precision is a measure of the relative calibration accuracy within the sample recorded. The absolute flux calibration is, in addition, affected by factors such as imperfections in the knowledge of the detector response and responsive transient correction, and differences between the spectral shapes of measured sources with respect to the canonical calibration source for ISOCAM, which has a stellar spectrum. Experience over many surveys suggests an absolute calibration accuracy of ±15% for ISOCAM faint-source photometry due to accumulated systematic effects. The measured colour ratios for the stars listed in Table 4 are consistent with this, and give some confidence in the absolute calibration at the ±15% level.

The number of sources in the primary and supplementary lists are 30 and 5, respectively, yielding a total of 35 sources. A search was performed for counterparts of the ISOCAM sources at other wavelengths, using a search radius of 6″ in HEASARC[6] and NASA/IPAC Extragalactic Database[7]. Of the 30 sources in the primary list (Table 2), 19 are identified with catalogued sources. Of these nineteen, four are stars, one is a quasar (PC 0023+1653), ten are cluster members, one is a foreground galaxy and three are background galaxies. As for the 5 supplementary sources (Table 3), three are identified with cluster galaxies. There is a total of 13 sources with unknown redshift and all have optical counterparts (Fig. 1).

[6] http://heasarc.gsfc.nasa.gov/db-perl/W3Browse/w3browse.pl

[7] The NASA/IPAC Extragalactic Database (NED) is operated by the Jet Propulsion Laboratory, California Institute of Technology, under contract with the National Aeronautics and Space Administration.

Table 5. References to ISOCAM sources in existing archives. The first column lists the source number from Tables 2 and 3. The key to the references in Cols. 2 to 8 is Dressler & Gunn (1992, DG), Czoske et al. (2001, CKS), Schneider et al. (1986, SDG), Smail et al. (1997, SDC), McLean & Teplitz (1996, MT), Butcher & Oemler (1978, BO), Soucail et al. (2000, S) and Pickles & van der Kruit (1991, P). The table does not include the four stars or the quasar PC 0023+1653.

id.	DG	CKS	SDG	SDC	MT	BO	Others
05	198	262	223			123	
06	278				64		
08	264	267	113		22	34	S01
09	257	282			6		
10	237	289					
12		381					
17	12						
18	47	444		797	4		
21	119	453					
22	43	459	146	834			
23	23			883			
24		471					
27	3	474		928			
1s	195	280			50		
3s	246	304			55		
4s	101	412	186	573	11	87	P61

The median flux-density of the unknown-redshift sources is about 250 μJy. The expected number of 15 μm sources lensed by the cluster down to that flux limit is about 20 ± 10, based on the log N – log S distribution of Metcalfe et al. (2003). So the expected number of background sources is sufficient to account for the observed number of unknown-redshift sources.

4.1. Spectral energy distributions

Spectral energy distributions were computed for the cluster galaxies using the 15 μm fluxes in Tables 2 and 3, and a 5σ upper limit of 400 μJy for the 7 μm fluxes. The spectral range of the ISOCAM sources was extended by including measurements in the optical photometric bands and the near-infrared. The values were retrieved from the NASA/IPAC Extragalactic Database. The references to extensive observations of the ISOCAM sources from a wide range of catalogues are listed in Table 5.

The SEDs were modelled using the program GRASIL (Silva et al. 1998). These models have already been used by Mann et al. (2002) to fit the SEDs of galaxies detected by ISOCAM in the *Hubble Deep Field South*. Given the limited photometric accuracy and, for some galaxies, the limited amount of available photometric data, it is not possible to obtain an accurate model of the SED of each individual galaxy. Instead, observed SEDs are compared with models representative of broad classes of spectral types. The number of models to be considered needs to be adequate to reflect the quality of the data and the questions to be answered (see, e.g., Rowan-Robinson 2003). The redshifts of the galaxies are known and hence it was possible to use more than the five models of Mann et al. (2002) without the risk of multiple solutions.

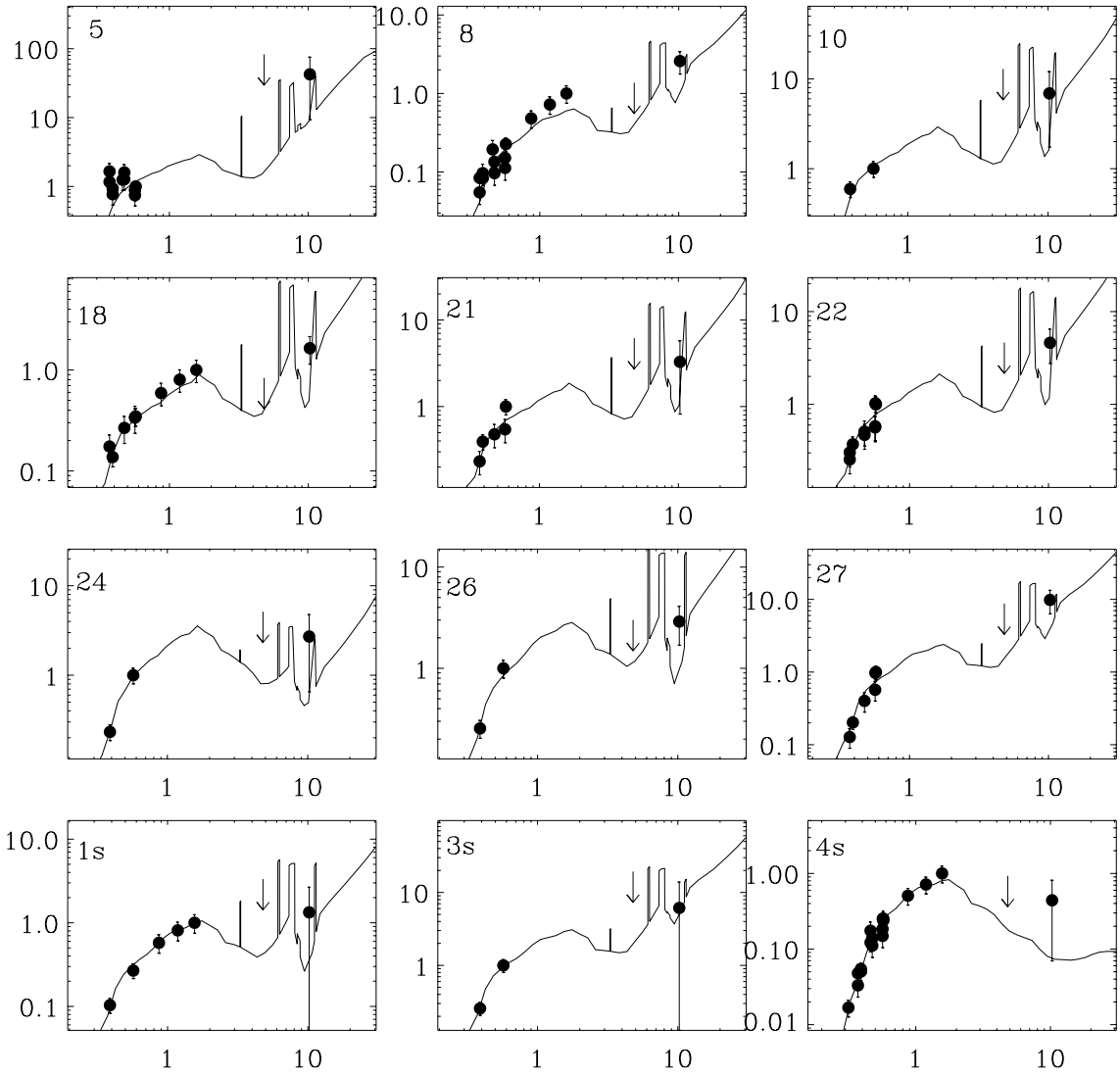

Fig. 3. SEDs for cluster members in Cl 0024+1654 detected at 15 μm. The horizontal axis is the wavelength in the cluster rest frame and the vertical axis is the flux density (in normalized units). The data points are given by black dots and the model fit to the SED by a continuous line.

In this work, 20 models were considered. They were taken from either the public GRASIL library, or built by running the publicly available GRASIL code, or kindly provided by L. Silva (private comm.). The 20 models reproduce the SEDs of several kinds of galaxies, from early-type, passively evolving ellipticals (labelled "E", in the following), to spiral galaxies (labelled "S"), and starburst galaxies (similar to the local examples Arp 220 and M 82), as seen either at the epoch of the starburst event, or 1 Gyr after (labelled "SB" or "SB+1", respectively). At variance with Mann et al. (2002) we avoid considering models older than the age of the Universe at the cluster redshift. Specifically, we consider models for galaxies with a formation redshift $z = 1$ (this is the redshift when stars start forming in the GRASIL models), corresponding to an age at the cluster redshift of ∼3 Gyr, and models with a formation redshift $z = 4$, corresponding to an age at the cluster redshift of ∼8 Gyr.

The best-fitting SED model was determined by χ^2 minimization, leaving the normalization of the model free. In principle, a given SED model cannot be freely rescaled, since the parameters in the GRASIL code depend on the mass of the galaxy. However, a fine tuning of the values of the GRASIL parameters only makes sense if the photometric uncertainties of the observed galaxy are small enough, and the SED is very well covered by observations, which is not the case here. As a matter of fact, the model SEDs of two galaxies of very different mass, such as M 82 and NGC 6090, could not be distinguished after rescaling, in the wavelength range covered by our observations, and with the accuracy of our photometric data points.

The SEDs are plotted in Fig. 3 and summarized in Table 6 for all cluster galaxies detected with ISOCAM, except for ISO_Cl0024_12, for which there are not enough photometric data. All the fits are acceptable at the 1% confidence level, and all, except two, at the 5% confidence level. S and SB+1 models provide the best-fit to most SEDs, but the fits are, in general, not unique. Among the acceptable fits (at the 5% confidence level) there are also SB and E models, but the latter always underestimate the mid-infrared fluxes. We are unable to distinguish between models with different formation redshifts.

Table 6. Results from model SEDs for known cluster galaxies in Cl 0024+1654. The columns list: LW3 identification number; best-fit SED model; number of data points in the observed SED; χ^2 of the fit; rejection probability of the fit; other acceptable models (rejection probability 95% or less); 15 μm k-correction; luminosity at 15 μm (h = 0.7, $\Omega_{\rm m}$ = 0.3, Ω_l = 0.7) using the transformation from Boselli et al. (1998), and k-corrected using best-fit SED; total infrared luminosity including the k-correction using the best-fit SED and computed using the transformation from Elbaz et al. (2002); SFR from total IR luminosity using the transformation of Kennicutt (1998); position in the $V-I$ vs. I colour–magnitude diagram (Fig. 7) where "MS" stands for "Main Sequence", "BO" for "Butcher-Oemler", "U" for "Unknown"; EW [O II] line from Czoske et al. (2001); SFR computed from the [O II] emission line using the transformation to the optical SFR; ratio infrared to optical SFR.

id.	Best-fit model	♯ of data points	χ^2	Rejection Probability	Other SED models	k-corr.	$L_{15\,\mu\rm m}$ ($L_\odot$)	$L_{\rm IR}$ ($L_\odot$)	SFR[IR] ($M_\odot\,{\rm yr}^{-1}$)	Colour Fig. 8	EW[O II] (Å)	SFR[O II] ($M_\odot\,{\rm yr}^{-1}$)	SFR[IR]/ SFR[O II]
05	S	12	17.8	96.2	None	1.45	2.03e+09	9.56e+10	16	U	–	–	–
08	SB+1	15	23.4	97.6	None	1.80	9.66e+09	4.54e+11	77	BO	–	–	–
10	S	4	1.9	79.8	S, SB+1	1.46	2.21e+09	1.04e+11	18	BO	–	–	–
18	S	11	3.9	13.4	E, S, SB+1	1.46	7.85e+09	3.69e+11	63	BO	–	–	–
21	S	7	5.4	74.7	SB+1, S	1.46	2.11e+09	9.93e+10	17	BO	–	–	–
22	S	11	7.6	52.6	S, SB+1	1.46	3.96e+09	1.87e+11	32	BO	17.5	4.9	6.5
24	S	4	1.2	79.8	E, SB+1, S	1.42	2.07e+09	9.74e+10	17	MS	5.0	0.8	21.3
26	S	4	1.4	79.8	S, SB+1	1.73	4.51e+09	2.17e+11	36	–	–	–	–
27	SB+1	8	6.7	87.8	SB	1.80	5.50e+09	2.59e+11	44	MS	–	–	–
1s	S	10	8.6	71.4	E, E, S, SB+1	1.73	1.96e+09	9.23e+10	16	BO	9.6	1.0	16.0
3s	SB+1	4	1.3	79.8	S, SB+1, E	1.80	1.59e+09	7.48e+10	13	MS	–	–	–
4s	E	20	9.4	7.3	E, S, SB+1	0.78	9.87e+08	4.66e+10	8	MS	–	–	–

Overall, the results show that most ISOCAM cluster sources have SEDs typical of actively star-forming galaxies, although not necessarily observed in an exceptional starbursting phase.

The SEDs of the nine cluster sources from the primary list were combined assuming the mean redshift of the ISOCAM cluster sources, and normalising the individual SEDs with the flux density in the rest-frame H band, either observed or as predicted by the best-fit SED models (see also Biviano et al. 2004). We did not consider the three supplementary sources; since their 15 μm flux values are rather uncertain, including these sources would increase the scatter of the average 15 μm flux density value. The resulting average observed SED is shown in Fig. 4, along with a SB+1 model fit to guide the eye (S models fit the average SED equally well). The average SED provides a synthetic view of the spectral shape of the 15 μm cluster galaxies, but we refrain from a physical interpretation of it, which would require a detailed analysis of the systematics inherent to its construction.

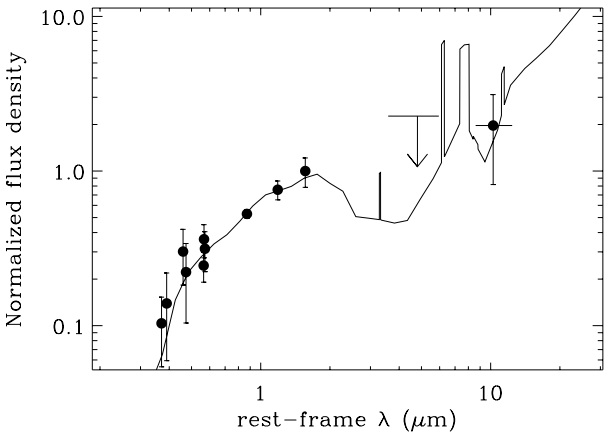

Fig. 4. The average SED of 9 ISOCAM cluster sources (the sources from the supplementary list have not been considered). Error bars give the rms values for the flux density. An upper limit of 400 μJy was used for $LW2$ at 7 μm. The solid line shows a model fit (SB+1) to the average SED.

4.2. Infrared and optical star formation rates for cluster members

The mid-infrared emission, free from dust extinction, is a reliable tracer of star formation (Genzel & Cesarsky 2000). The infrared emission from a galaxy is the sum of various contributions including:

1) continuum emission from dust particles;
2) line emission from carriers of Unidentified Infrared Bands (UIBs);
3) line emission from ionized interstellar gas;
4) emission from the evolved stellar population that dominates early-type galaxies;
5) non-thermal emission from radio sources.

The infrared spectrum of a galaxy depends on its morphological type and evolutionary status. For elliptical galaxies, the spectrum is similar to a blackbody continuum at a temperature of 4000–6000 K with a [7 μm]/[15 μm] flux ratio of about 4.5, while for spiral galaxies the ratio of the [7 μm]/[15 μm] flux is around 1 (Boselli et al. 1998). Starburst galaxies are characterized by a rapid increase in emission towards 15 μm because of the contribution from very small grains, which are dust particles with radii of ∼10 nm that are abundant in star forming regions (Laurent et al. 2000).

The luminosities at 15 μm, in units of solar luminosity, were obtained using the relationship (Boselli et al. 1998):

$$L_{15\,\mu\rm m} = 4\,\pi\,{D_{\rm L}}^2\,F_{15\,\mu\rm m}\,\delta_{15\,\mu\rm m} \quad (1)$$

where $F_{15\mu\rm m}$ is the flux at 15 μm in mJy and $\delta_{15\,\mu\rm m} = 5.04 \times 10^{12}$ Hz is the bandwidth of the $LW3$ filter. The total

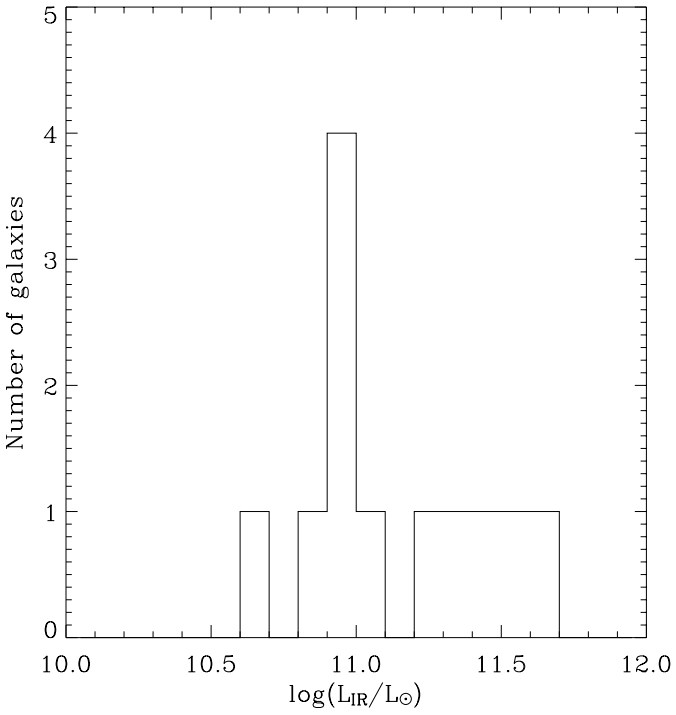

Fig. 5. The total infrared luminosity distribution for cluster members. The median value for $L_{\rm IR}$ is $\sim 1.0 \times 10^{11}\ L_\odot$.

(8−1000 μm) infrared luminosity was obtained from the empirical relation of Elbaz et al. (2002):

$$L_{\rm IR} = 11.1^{+5.5}_{-3.7} \times (\nu\, L_\nu[15\,\mu{\rm m}])^{0.998}. \quad (2)$$

The total IR emission was also obtained directly from the best-fit SED model and provides an alternative determination of the total infrared luminosity. The total IR luminosities obtained from the two methods were compared and found to agree to within 32%. We adopt the IR luminosities obtained from Eq. (2) for the cluster galaxies. The luminosities are listed in Table 6 and include the k-corrections obtained from the best-fit SEDs. Depending on the best-fit model, the k-correction at the cluster redshift ranges from 0.8 to 1.8 with a median (mean) of 1.5 (1.5). The distribution of the total infrared luminosities for cluster galaxies is given in Fig. 5. The mid-infrared cluster members have total IR luminosities between $4.7 \times 10^{10}\ L_\odot$ and $4.5 \times 10^{11}\ L_\odot$, with a median value of $1.0 \times 10^{11}\ L_\odot$. Six of the 12 galaxies have total infrared luminosities above $10^{11}\ L_\odot$, which classify them as LIRGs ($10^{11}\ L_\odot \le L_{\rm IR} \le 10^{12}\ L_\odot$, e.g. Genzel & Cesarsky 2000), and four more have infrared luminosities above $9 \times 10^{10}\ L_\odot$. The star formation rates in units of solar masses per year, SFR[IR], were derived using the relation of (Kennicutt 1998):

$$SFR[{\rm IR}] \simeq 1.71 \times 10^{-10}\ (L_{\rm IR}/L_\odot). \quad (3)$$

The values of SFR[IR] are listed in Table 6. The infrared SFRs range between $\simeq 8\ M_\odot\,{\rm yr}^{-1}$ and $\simeq 77\ M_\odot\,{\rm yr}^{-1}$, with a median (mean) value of 18 (30) $M_\odot\,{\rm yr}^{-1}$.

Half of the 15 μm cluster galaxies are LIRGs and four more are within 1σ of the luminosity of a LIRG. Star forming episodes that are enshrouded by dust are commonly found in these galaxies in the field. The cause of the starburst phase of LIRGs in the local universe is still debated, but in the range of infrared luminosities measured with ISOCAM the starburst seems to be linked to mergers or interactions between pairs of spiral galaxies of unequal size and single galaxies in about one-quarter of the sources (Hwang et al. 1999; Ishida & Sanders 2001). The cause of the starburst in the 15 μm sources of Cl 0024+1654 seems to be consistent with what is observed in the local universe because of the evidence for interactions and mergers in the HST maps (see Sect. 5.2). The [O II] line is often used to determine the SFR in galaxies at intermediate redshift, when the Balmer hydrogen lines are outside the spectral range (e.g. Barbaro & Poggianti 1997; Jansen et al. 2000). There are several problems associated with this line. [O II] is subject to dust extinction, and its strength depends heavily on the metallicity and ionization of the interstellar medium (Kennicutt 1998; Jansen et al. 2000). Furthermore, Balmer lines are more correlated to UV emission from young stars than [O II]. Therefore, the uncertainties in SFR computed from [O II] are very large. Nevertheless, there may be times when it is the only indicator available, in which case finding ways to correct the determination for dust extinction will be important. It may well yield only a lower limit on the SFR.

The Equivalent Width (*EW*) of the [O II] line was available from Czoske et al. (2001) for only three of the mid-infrared cluster members. The [O II] line is redshifted into the *V* band and can be used to compute the optical SFR provided that the *V*-band magnitude is known. The luminosity L_ν was derived from the *V*-band magnitude in units of erg s^{-1} Å^{-1} using:

$$L_V = 4\,\pi\, D_L^2 \times (3.08 \times 10^{24})^2 \times 10^{-0.4 m_v} \times 3.92 \times 10^{-9} \quad (4)$$

where D_L is in Mpc and m_v is the apparent magnitude in the *V*-band. The luminosity of the [O II] line is given by $L[{\rm O\,II}] = EW[{\rm O\,II}] \times L_V$ in units of erg s^{-1}. Finally, the SFR was obtained using $SFR[{\rm O\,II}] \sim 1.4 \times 10^{-41}\ L[{\rm O\,II}]$, in units of $M_\odot\,{\rm yr}^{-1}$ (Kennicutt 1998). The SFRs derived from the EWs of the [O II] lines are listed in Table 6 and should be regarded as lower limits because no correction for extinction was applied. The mean value of the optical SFR is 2.2 $M_\odot\,{\rm yr}^{-1}$ and increases to 3 $M_\odot\,{\rm yr}^{-1}$ when the canonical value of 1 mag at Hα (Kennicutt 1992), for extinction in the optical, is applied. The values of SFR[O II] show a wide range, and are sometimes more than 1 order of magnitude lower than those obtained in the infrared. Recent data show that there is a better agreement when the SFRs are computed from the Hα line and the mid-infrared (Kodama et al. 2004). The ratios of SFR[IR]/SFR[O II] range from 7 to 21 with a median value of 16 (Sect. 4.2). Therefore the vast bulk of the star formation is missed when the [O II] line emission is used. A large fraction of the star formation in Cl 0024+1654 is enshrouded by dust (see Cardiel et al. 2003 for a thorough discussion on the comparison of SFR-estimators). Duc et al. (2002) and Balogh et al (2002) have arrived at a very similar conclusion for the cluster Abell 1689, which has many mid-infrared sources. Similar results have also been obtained for field galaxy samples (see, e.g., Charlot et al. 2002).

In our sample, AGN activity does not seem to be a major contributor to the energy output of the systems. Measurements

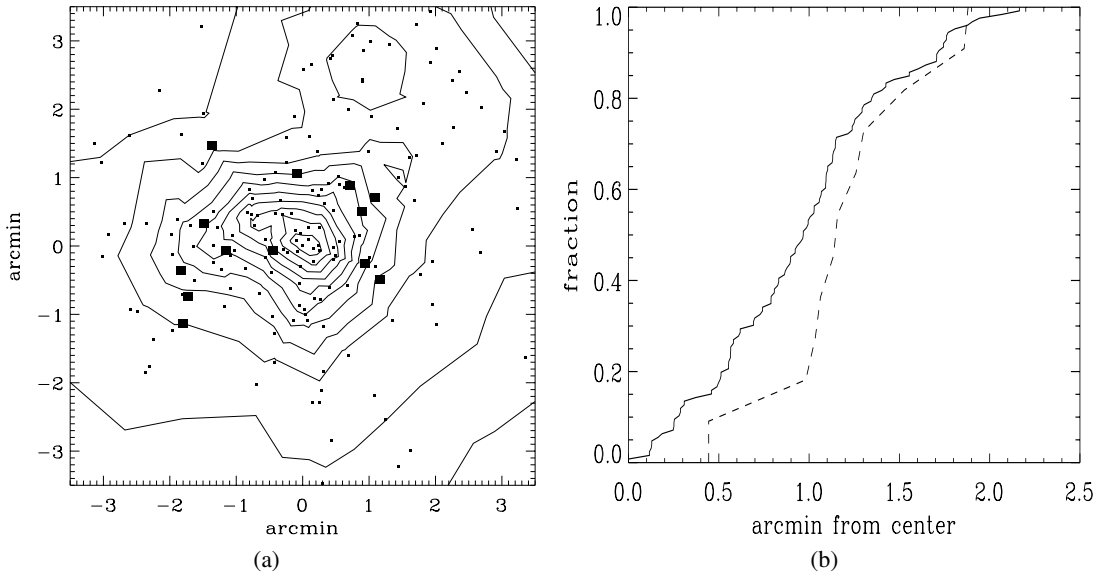

Fig. 6. a) Adaptive Kernel map for cluster members. Black boxes represent the 15 μm sources while dots and isodensity contours trace the distribution of component-A galaxies. **b)** Radial distribution from the centre of component-A galaxies (continuous line) and 15 μm cluster galaxies (dashed line) within the region covered by the ISOCAM observations.

of the Hα and [N II] emission lines are required to further determine the AGN contribution to the mid-infrared emission (Balogh et al. 2002) and future radio observations could also help in determining the AGN contribution (Rengarajan et al. 1997; Dwarakanath & Owen 1999).

5. Spatial, dynamical and colour properties of the 15 μm cluster galaxies

5.1. Spatial and velocity distributions

The spatial and radial distributions of the cluster galaxies, with and without detectable 15 μm emission, are given in Fig. 6. The isodensity contours and dots in Fig. 6a refer to galaxies belonging to component A, while the black boxes represent the cluster members with 15 μm emission. The figure shows that the cluster members detected at 15 μm are less concentrated than the cluster galaxies not detected in the mid-infrared. The Kolmogorov-Smirnov test reveals that there is only a 4% probability that the two distributions are drawn from the same parent one.

The velocity distributions for cluster galaxies with and without detectable 15 μm emission are given in Fig. 2. The counterparts of the 15 μm sources have redshifts which place them in Component A – the larger of the two interacting components. One source, ISO_Cl0024_12, with $z = 0.386$ is close to the boundary. The velocity dispersion computed in the cluster rest-frame (Fig 2), using the biweight estimator (Beers et al. 1990) in the central region of the ISO map, is $\sigma_v = 914^{+59}_{-56}$ km s^{-1} for a sample of galaxies, while it is $\sigma_v = 979^{+238}_{-193}$ km s^{-1} for the 15 μm galaxies. The 15 μm sources are associated mainly with spiral and emission-line galaxies, and studies of nearby clusters indicate a larger velocity distribution for this population relative to the general cluster population (Biviano et al. 1997).

5.2. Colour–magnitude diagramme

The colour–magnitude diagramme for cluster galaxies is given in Fig. 7. It provides an important link between the optical and mid-infrared properties of the ISOCAM galaxies. Apparent magnitudes in the V and I bands are available from Czoske et al. (2001) for 11 of the 13 ISOCAM cluster galaxies. The circles represent component-A galaxies within the region mapped by ISOCAM. The spectroscopically confirmed mid-infrared cluster galaxies are indicated by filled circles and are labelled with the ISO source number. Section M of Fig. 7 contains the galaxies that satisfy the BO definition, given in Sect. 1. Six of the 15 μm galaxies fall in section M and satisfy the BO requirement. Only 20% of the cluster galaxies in section M are detected at 15 μm. However, this fraction increases to ~38% when only galaxies brighter than $m_I = 19.8$ are considered. The non-detections of fainter I-band sources are probably due to the sources falling below the sensitivity limits of ISOCAM.

All 15 μm cluster sources have in common an excess of mid-infrared emission that sets them apart from the rest of the cluster members. In at least some of these systems, one would expect that the star forming activity is primarily triggered by interactions and mergers. Recent changes in the galaxy population reveal themselves in the mid-infrared and help identify the processes that cause the burst of obscured star formation. The infall of smaller groups into the cluster environment provides a way of promoting slow encounters and mergers within clusters (Mihos 2004). Slow encounters between galaxies are better able to drive instabilities than fast encounters. Complex interactions of the kind that may occur between galaxies in this cluster have been studied in the local Universe in Hickson Compact Groups (see, e.g., López-Sánchez et al. 2004, and references therein).

We looked for indications of ongoing and past interaction events among the 15 μm cluster sources, either in their

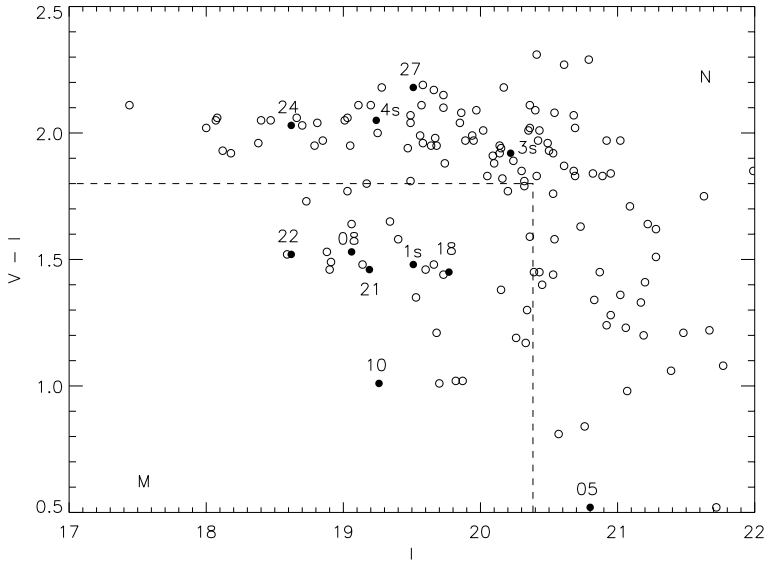

Fig. 7. $V-I$ colour–magnitude diagramme for component-A galaxies (empty circles) within the region mapped by ISOCAM. The eleven 15 μm cluster galaxies (filled circles) are identified by their ISO source number from Tables 2 and 3. The V and I magnitudes were not available for source ISO_Cl0024_12. The galaxies in section M, which is defined by $V-I<1.8$ and I < 20.4, are BO galaxies. Surprisingly, five of the 15 μm sources are in section N and not associated with BO galaxies.

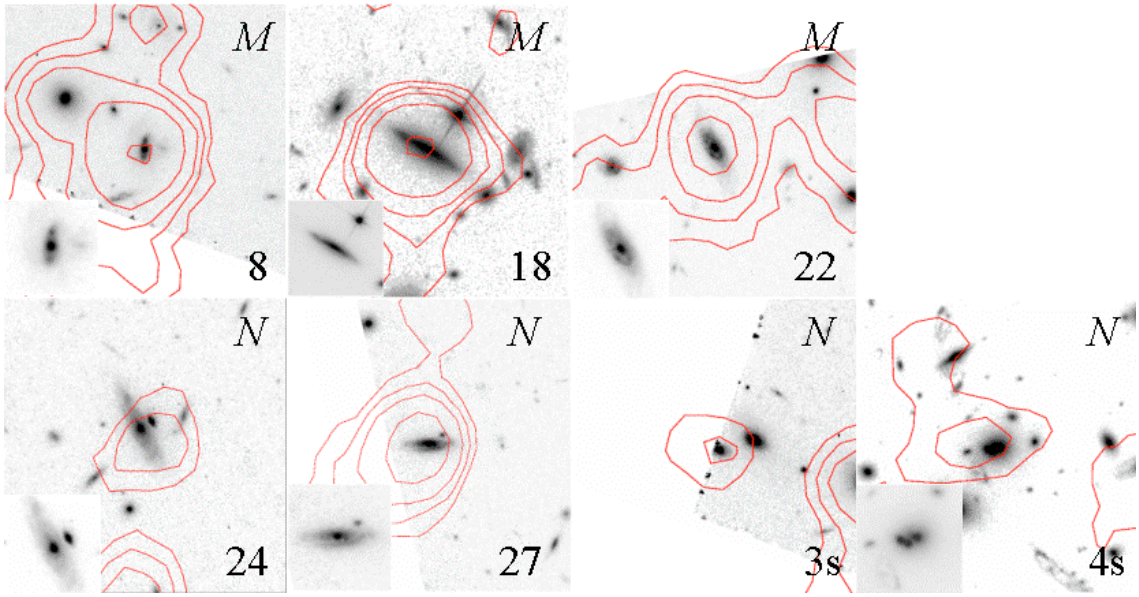

Fig. 8. Miniature maps obtained from HST. The maps are centred on the 15 μm source coordinates and labelled with the source number in Tables 2 and 3. The letters M and N at the top right of the images give the positions of the cluster sources in the colour–magnitude diagramme (Fig. 7). All images are 30×30 arcsec^2. Insets show details of the optical counterpart. North is up, East to the left.

morphologies, or in their spectra. A HST image was available for part of Cl 0024+1654 from the MORPHS collaboration (Smail et al. 1997). This image is limited to the South-Eastern region of the cluster core and contains seven of the 15 μm cluster sources. For these galaxies, miniature maps centred on the ISOCAM source coordinates and having an area of 30×30 arcsec^2 were obtained. The miniature maps are presented in Fig. 8.

Miniature maps are available for 3 of the BO galaxies in section M of Fig. 7. The HST maps show that ISO_Cl0024_18 and ISO_Cl0024_22 do not have companions within a radius of 5″ while ISO_Cl0024_08 appears to be interacting with at least another galaxy.

HST miniature maps for four of the non-BO 15 μm emitters in section N are also given in Fig. 8 and each has at least one nearby companion. ISO_Cl0024_4s appears to be merging because it has multiple nuclei and has at least two other companions. ISO_Cl0024_24 and ISO_Cl0024_3s show evidence of ongoing interactions (e.g. tidal bridges) with at least one nearby galaxy.

Even though the number of infrared sources with HST maps is small, there seems to be a difference between

Table 7. Summary of ISOCAM observations and results at 15 μm for five clusters of galaxies. The data was obtained from Metcalfe et al. (2003) for Abell 370, Abell 2218 and Abell 2390, Fadda et al. (2000) and Duc et al. (2002) for Abell 1689, and this paper for Cl 0024+1654. The content of the columns in the table are as follows: name and redshift of the cluster, total area scanned, sensitivity reported at the 5σ level, flux of the weakest reported source in μJy, total observation time, total number of sources detected including sources without redshifts and stars. Then number of cluster galaxies, virial radius, virial mass, number of sources with $L_{\rm IR} > 9 \times 10^{10}\ L_\odot$ detected and expected. The expected number of sources was obtained by comparison with Cl 0024+1654 as described in the text. Virial radii and masses are from Girardi & Mezzetti (2001) and King et al. (2002).

Cluster	z	Area	Sensitivity	Faintest source	Obs. t.	Tot. n.	Cluster	$R_{\rm vir}$	$M_{\rm vir}$	$N_{\rm comp}$	
		($'^2$)	(5σ)	(μJy)	(s)	sources	galaxies	(h^{-1} Mpc)	($h^{-1}\ 10^{14}\ M_\odot$)	Detected	Expected
Cl 0024	0.39	37.8	140	141	22615	35	13	0.94	6.42	10	–
A 370	0.37	40.5	350	208	22688	20	1	0.91	5.53	1	8
A 1689	0.18	36.0	450	320	9500	18	11	1.1	5.7	0	1
A 2390	0.23	7.0	100	54	29300	28	4	1.62	20.35	0	1
A 2218	0.18	20.5	125	90	22000	46	6	1.63	18.27	0	1

the BO and non-BO galaxies in the sense that the former tend not to have nearby companions whereas the latter do. The optical counterparts of the 15 μm sources on the main colour–magnitude sequence are not passive early type galaxies as one would expect from their position in the colour–magnitude diagramme. Rather, the optical counterparts appear to be galaxies that are involved in interactions and mergers in the HST images.

There is indirect support for this apparent difference between the BO and non-BO galaxies from the results of the SED fitting process. Five of the six 15 μm galaxies in the BO region of the diagram have SEDs that are best-fit by S-type models. On the other hand, two out of four 15 μm galaxies on the main sequence of the colour–magnitude diagram have SEDs that are best-fit by SB+1-type. If the starburst events are triggered by interactions, there is marginal evidence from the SED analysis that the 15 μm galaxies on the main colour–magnitude sequence have suffered more interaction events in the recent past than the BO 15 μm galaxies.

Given the scarce morphological data, and the fact that the SED fitting results are not very well constrained (SB+1-type models also provide acceptable fits to the SEDs of BO galaxies, see Table 6), we consider the evidence for a difference in the interaction properties of BO and non-BO 15 μm galaxies only tentative. We conclude from our data that interaction events do trigger the star formation activity (and stimulate the IR emission) in at least some 15 μm cluster galaxies.

Obscuration by dust could explain why some 15 μm sources lie on the cluster main sequence. We tested this possibility by computing the de-reddened V and I magnitudes of the 15 μm galaxies, using the dust-free best-fit model SEDs, as given by the GRASIL code. As expected, once de-reddened the 15 μm galaxies on the colour–magnitude sequence move in the colour–magnitude diagramme toward the BO region, and in one case (ISO_Cl0024_3s), it even becomes part of the BO category (Fig. 7). Dust obscuration at least partially explains the unusual colours of the 15 μm sources on the cluster main sequence.

6. Comparison of Cl 0024+1654 with other clusters observed by ISO

Observations of clusters of galaxies at high redshift ($z > 0.4$) with SCUBA have yielded an excess of sub-millimeter sources with high values of the SFR (Best 2002). Here we compare the results of the observations of Cl 0024+1654 with four clusters of galaxies that were observed with ISOCAM at 15 μm (Fadda et al. 2000; Metcalfe et al. 2003) to determine if Cl0024+1654 has more LIRGs than the other clusters. We have not included the cluster J 1888.16 Cl in Table 7 because the relevant data have not been published (Duc et al. 2004). However this cluster seems to be comparable to Cl0024+1654 because it has many infrared sources and at least 6 of them are confirmed LIRGs. The characteristics of the observations, and results for the five clusters, are summarized in Table 7. The observed areas and sensitivities are comparable for the first three clusters in Table 7, but the area is somewhat smaller for Abell 2218, and much smaller for the ultra-deep observations of Abell 2390.

The number of 15 μm sources that are identified with cluster galaxies ranges from 13 in Cl 0024+1654 to 1 in Abell 370. The number of 15 μm sources that have fluxes consistent with LIRGs, within the precision of the measurements is listed in Table 7. In Cl 0024+1654 the number of LIRGs is 10 (Table 7) and includes 6 sources with $L_{\rm IR} \geq 10^{11}\ L_\odot$ and 4 more with $L_{\rm IR}$ between $9 \times 10^{10}\ L_\odot$ and $1 \times 10^{11}\ L_\odot$ (Table 6). The number of LIRGs detected in the other clusters is either 0 or 1 (Table 7). The virial mass and radius of Cl 0024+1654, Abell 370 and Abell 1689 are the same to within 20% and are considerably smaller than the values for the more massive clusters Abell 2218 and Abell 2390.

However the ratio of the virial mass to area within the virial radius varies by less than 50% for the 5 clusters. We now compare the number of LIRGs in Cl 0024+1654 with those in the other clusters. The comparison is limited to LIRGs because it eliminates selection effects for the 15 μm sources. In any case most of the 15 μm sources in the nearer clusters are too faint to be detected in the more distant clusters Cl 0024+1654

and Abell 370. In the comparison, the number of LIRGs in Cl 0024+1654 was multiplied by the ratios of:

a) the virial mass per unit area (since cluster mass is approximately proportioned to richness – see Bahcall & Cen 1993) of the cluster to that of Cl 0024+1654;
b) the square of the distance to the cluster and that to Cl 0024+1654;
c) the observed solid angle of the cluster to that of Cl 0024+1654.

The values are listed in the last column of Table 7. The simple scaling of the mapped area will not be sufficient if the infrared galaxies have a spatial distribution that is different from the overall cluster population. In particular the mapped regions of the three nearer clusters (Abell 1689, Abell 2218, Abell 2390) are smaller and more confined to the central regions than the two more distant clusters (Abell 370 and Cl 0024+1654). The infrared sources could preferentially occur in the peripheral regions of clusters where dynamical interactions between galaxies may be more effective in triggering interactions and bursts of star formation (Mihos 2004). In this case, the LIRG populations for the complete clusters may in some cases be less different than the regions currently mapped would make it appear. Future observations with Spitzer are needed to address this possibility (Werner et al. 2004).

6.1. LIRGs in Cl 0024+1654 and Abell 370

The clusters Cl 0024+1654 and Abell 370 have comparable redshifts and were observed by ISOCAM with almost identical observational parameters, such as, on-chip integration time, total area observed in raster mode, and total observation time. The total number of cluster sources in Cl 0024+1654 is 13 whereas the corresponding number is 1 for Abell 370 (Table 7). The observed number of LIRGs in Abell 370 is only 1 whereas 8 were expected from the comparison with Cl 0024+1654. There is a real difference between the populations of LIRGs and also in the ratio of the mass to infrared light for the two clusters. No LIRGs were detected in the three clusters Abell 1689, Abell 2218 and Abell 2390 at lower redshifts whereas a total number of 3 was expected from the comparison with Cl 0024+1654. A population of luminous infrared galaxies is also absent from the central regions of the Coma and Virgo clusters (Boselli et al. 1997, 1998; Quillen et al. 1999; Leech et al. 1999; Tuffs et al. 2002a, 2002b).

6.2. Mid-infrared sources in Abell 1689 and Abell 2218

It is, further, interesting to compare the two clusters Abell 1689 and Abell 2218 that are at the same redshift. The observations of Abell 2218 are more sensitive to 15 μm sources than those of Abell 1689 (Table 7). However there is no significant difference between the total number of 15 μm sources when allowance is made for the scanned area and virial mass per unit area. The difference caused by the sensitivity of the observations is revealed by a comparison of the median fluxes of the 15 μm sources which is ~600 μJy for Abell 1689 and ~150 μJy for Abell 2218. All of the 15 μm sources in Abell 1689 would have been easily detected in Abell 2218, if present, whereas only one of the sources in Abell 2218 might have been detected in the Abell 1689 measurement. The 15 μm sources detected in Abell 2218 have lower fluxes and luminosities than those in Abell 1689 and this effect is not caused by the sensitivities of the observations of the two clusters. It is very interesting that Abell 1689 and Abell 2218 follow the same trend identified in the comparison between Cl 0024+1654 and Abell 370.

Large numbers of cluster sources are detected by ISOCAM at 7 μm in both Abell 1689 and Abell 2218. In Abell 2218 the SEDs of most of these 7 μm sources are well fit by models of quiescent ellipticals with negligible SFRs and a median luminosity of $\sim 6 \times 10^8\ L_\odot$ (Biviano et al. 2004).

6.3. Dynamical status of clusters and population of mid-infrared sources

Cl 0024+1654 is involved in a recent merger, as shown by the two velocity components in Fig. 2. Abell 1689 also has a complex and broad velocity structure, with evidence for three distinct groups that overlap spatially and are well separated in velocity space (Girardi et al. 1997). The two clusters Abell 370 and Abell 2218 show no evidence for major merger activity. The number of luminous 15 μm sources can be, in part, explained by considering the dynamical status of the cluster. Simulations made by Bekki (1999) show that the time-dependent tidal gravitational field existing in cluster-group mergers induces secondary starbursts by efficiently transferring large amounts of gas from the disk to the nucleus. The model establishes a link between the population of starburst or post-starburst galaxies and the presence of substructures in clusters. The existence of starburst and post-starburst galaxies in a merging cluster, and spread over a wide area, is an important prediction of this model which seems to be in agreement with the results from Cl 0024+1654 and Abell 1689.

Furthermore it can be expected that merging clusters at much larger redshifts than Cl 0024+1654 will contain LIRGs and ULIRGs because the interacting and merging galaxies will be more gas rich (see, e.g. Balogh et al. 2000; Kauffmann & Haehnelt 2000; Francis et al. 2001).

In this context it is interesting to note that Dwarakanath & Owen (1999) found different radio source populations in two very similar clusters. The number density of radio sources in Abell 2125 ($z = 0.246$) exceeded that in Abell 2645 ($z = 0.25$) by almost an order of magnitude. The cluster Abell 2125, with the larger number of radio sources, also shows evidence for a merger.

6.4. Mid-infrared sources in Cl 0024+1654 and Abell 1689

Many infrared sources were found in the cluster Abell 1689 (Fadda et al. 2000) that is at a much smaller redshift than Cl 0024+1654. No galaxy in Abell 1689 has total infrared luminosity above $1 \times 10^{11}\ L_\odot$ (we use our cosmology and Eq. (2) to convert the 15 μm fluxes from Fadda et al. (2000) to total infrared luminosities), while half of the 15 μm cluster sources

in Cl 0024+1654 are above this luminosity. All of the 15 μm sources detected in Cl 0024+1654 would have been easily detected in Abell 1689, if present, whereas most of the sources in Abell 1689 would not have been detected in the observations of Cl 0024+1654 when allowance is made for different sensitivities and distances. The two clusters have very similar virial radii and masses (Table 7). However a much larger part of the periphery of Cl 0024+1654 was observed because it is at a higher redshift. It is possible that some of the differences between the 15 μm sources arises from a change in the source population between the core and periphery of the two clusters.

The population of 15 μm sources may also be influenced by the history of the cluster. Various processes such as ram pressure stripping of gas from cluster galaxies, tidal effects and previous starbursts will inevitably leave less gas in the interacting and merging galaxies to fuel the starburst (e.g. Gunn & Gott 1972; Byrd & Valtonen 1990; Fujita 1998). These processes may vary from one cluster to another depending on its history and provide dispersion in the luminosity of the starbursts. The large number of LIRGs in Cl 0024+1654 are fuelled by the gas rich progenitor galaxies. It is conceivable that in Abell 1689 the starbursts are less luminous either because there is a smaller supply of gas to fuel the outburst, or the luminosity has decreased because a longer time has elapsed since the last merger or there is a significant difference between the sources in the core and periphery.

The average value of the ratio SFR[IR]/SFR[O II] is reasonably comparable for both clusters (it is ∼15 for Cl 0024+1654 and ∼11 for Abell 1689). The internal properties of the 15 μm sources in Cl 0024+1654 and Abell 1689 are broadly similar even though their distributions of the luminosities of 15 μm sources are different. The colour–magnitude diagrammes of the 15 μm sources in the two clusters are also quite similar.

7. Conclusions

The cluster Cl 0024+1654 was observed with ISO. A total of 35 sources were detected at 15 μm and all have optical counterparts. Sources with known redshift include four stars, one quasar, three background galaxies, one foreground galaxy and thirteen cluster galaxies. The remaining 13 sources are likely to be background sources lensed by the cluster.

The spatial, radial and velocity distributions were obtained for the cluster galaxies. The ISOCAM cluster galaxies appear to be less centrally grouped (in the cluster) than those not detected at 15 μm and the Kolmogorov-Smirnov test reveals that there is only a 4% probability that the two distributions are drawn from the same parent population. No statistically significant differences were found between the velocity distributions of the 15 μm sources and other cluster galaxies in the region mapped by ISOCAM.

Spectral energy distributions were obtained for cluster members and used as indicators of both morphological type and star forming activity. The ISOCAM sources have as best-fit SEDs predominantly those of spiral or starburst models observed 1 Gyr after the main starburst. Star formation rates were computed from the infrared and the optical data. The SFRs inferred from the infrared are one to two orders of magnitude higher than those computed from the [O II] line emission, suggesting that most of the star forming activity is hidden by dust.

A colour–magnitude diagramme is given for cluster sources falling within the region mapped by ISOCAM. V and I-band magnitudes are available for 11 of the cluster sources, and 6 of these have colour properties that are consistent with Butcher-Oemler galaxies and best-fit SEDs that are typical of spiral models. The remaining 15 μm cluster galaxies have colours that are not compatible with Butcher-Oemler galaxies and have best-fit SEDs that are typical of starburst galaxies 1 Gyr after the main burst. HST images are available for these latter systems and all have nearby companion galaxies. These results suggest that interactions and mergers are responsible for some of the luminous infrared sources in the cluster.

The 15 μm sources in Cl 0024+1654 were compared with four other clusters observed with ISOCAM. The results show that the number of LIRGs in Abell 370 is smaller than expected by about one order of magnitude, if Abell 370 were to be comparable with Cl 0024+1654. Furthermore no LIRGs were detected in Abell 1689, Abell 2218 and Abell 2390 when a total of 3 was expected, based on the results from Cl 0024+1654. A comparison of the mid-infrared sources in Abell 1689 and Abell 2218 shows that the sources in Abell 1689 are more luminous than in Abell 2218 and follow the same trend identified in the comparison between Cl 0024+1654 and Abell 370. There is clear evidence for an ongoing merger in Cl 0024+1654 and Abell 1689. The number and luminosities of the mid-infrared cluster sources seem to be related to the dynamical status and history of the clusters.

Acknowledgements. D.C. and B.McB. thank Enterprise Ireland for support. We thank Laura Silva for valuable discussions regarding the spectral energy distributions. We also thank T. Treu and S. Moran for redshift informations. D.C. gratefully acknowledges the hospitality of ESA's ISO Data Centre (IDC) at Vilspa, Spain, where part of this work was completed. JPK acknowledges support from CNRS as well as from Caltech. The ISOCAM data presented in this paper was analysed using "CIA", a joint development by the ESA Astrophysics Division and the ISOCAM Consortium. The ISOCAM Consortium is led by the ISOCAM PI, C. Cesarsky. We thank the anonymous referee for the many comments that improved the content of the paper.

Appendix A: Additional notes on some mid-infrared sources

ISO_Cl0024_02 Radio quiet quasar PC 0023+1653 (Schmidt et al. 1986) at a redshift of 0.959 with an X-ray luminosity $L_X = 1.4 \times 10^{44}$ erg s^{-1} (Soucail et al. 2000).

ISO_Cl0024_04 The 15 μm map has two bright regions that may contain contributions from two optical counterparts. There are no measured redshifts.

ISO_Cl0024_06 The 15 μm emission appears to have contributions from various galaxies in the field-of-view. No redshifts are available for these sources.

ISO_Cl0024_10 Most of the 15 μm emission is centred on a cluster galaxy at redshift $z = 0.400$ (Table 2), the brightest of the two galaxies in Fig. 8. The model fit to the SED is an Sc (Fig. 3). The source was also detected in X-rays

with ROSAT (Böhringer et al. 2000). The optical identification for the ROSAT source is uncertain because there are two sources in the error box. One of the sources is a typical cluster galaxy while the second is a star-forming foreground galaxy ($z = 0.2132$). The cluster galaxy is closer to the 15 μm coordinates and was adopted as the mid-infrared counterpart. It is the only cluster AGN detected so far in Cl 0024+1654.

ISO_Cl0024_16 The redshift of the optical counterpart on the VLT image is not known. The 15 μm emission is centred on one galaxy and partially extends to two very faint optical sources that are north of the main optical source.

ISO_Cl0024_17 The redshift of the optical counterpart on the VLT image has not been measured. The 15 μm emission is centred on the bright optical source and is partially elongated towards two other sources on the VLT map.

ISO_Cl0024_18 The optical counterpart is a large, edge-on, late type, cluster spiral galaxy. The 15 μm emission is centred on the galaxy and has contributions from several other sources. The HST image reveals a disturbance of the spiral structure.

ISO_Cl0024_22 The optical counterpart is a cluster galaxy with $z = 0.3935$. The HST image (Fig. 8) reveals a spiral galaxy with an inner ring, a smoother outer arm (Smail et al. 1997) and bright knots.

ISO_Cl0024_23 The redshift of the optical counterpart is not available. At the 15 μm coordinates, the HST image shows two interacting spiral galaxies and a tidal arm.

ISO_Cl0024_30 The source is outside the boundaries of the VLT and HST images (Fig. 1) and has a faint optical counterpart (Fig. 4d in Czoske et al. 2001).

References

Abraham, R. G., van den Bergh, S., Glazebrook, K., et al. 1996a, ApJS, 107, 1

Abraham, R. G., Smecker-Hane, T. A., Hutchings, J. B., et al. 1996b, ApJ, 471, 694

Altieri, B., Metcalfe, L., Kneib, J. P., et al. 1999, A&A, 343, L65

Aussel, H., Vigroux, L., Franceschini, A., et al. 1999, BAAS, 31, 1386

Bahcall, N. A., & Cen, R. 1993, ApJ, 407, L49

Balogh, M. L., Navarro, J. F., & Morris, S. L. 2000, ApJ, 540, 113

Balogh, M. L., Couch, W. J., Smail, I., Bower, R. G., & Glazebrook, K. 2002, MNRAS, 335, 10

Barbaro, G., & Poggianti, B. M. 1997, A&A, 324, 490

Beers, T. C., Flynn, K., & Gebhardt, K. 1990, AJ, 100, 32

Bekki, K. 1999, ApJ, 510, L15

Bertin, E., & Arnouts, S. 1996, A&AS, 117, 393

Best, P. N. 2000, MNRAS, 317, 720

Best, P. N. 2002, MNRAS, 336, 1293

Biviano, A., Katgert, P., Mazure, A., et al. 1997, A&A, 321, 84

Biviano, A., Metcalfe, L., McBreen, B., et al. 2003, Mem. Soc. Astron. Ital., 74, 266

Biviano, A., Metcalfe, L., McBreen, B., et al. 2004, A&A, in press

Böhringer, H., Soucail, G., Mellier, Y., Ikebe, Y., & Schuecker, P. 2000, A&A, 353, 124

Boselli, A., Lequeux, J., Contursi, A., et al. 1997, A&A, 324, L13

Boselli, A., Lequeux, J., Sauvage, M., et al. 1998, A&A, 335, 53

Broadhurst, T., Huang, X., Frye, B., & Ellis, R. 2000, ApJ, 534, L15

Butcher, H., & Oemler, A. 1978, ApJ, 219, 18 (BO)

Butcher, H., & Oemler, A. 1984, ApJ, 285, 426

Byrd, G., & Valtonen, M. 1990, ApJ, 350, 89

Cardiel, N., Elbaz, D., Schiavon, R. P., et al. 2003, ApJ, 584, 76

Cesarsky, C. J., Abergel, A., Agnese, P., et al. 1996, A&A, 315, L32

Charlot, S., Kauffmann, G., Longhetti, M., et al. 2002, MNRAS, 330, 876

Coia, D., Metcalfe, L., McBreen, B., et al. 2005, A&A, 430, 59

Colley, W. N., Tyson, J. A., & Turner, E. L. 1996, ApJ, 461, L83

Contursi, A., Boselli, A., Gavazzi, G., et al. 2001, A&A, 365, 11

Couch, W. J., Barger, A. J., Smail, I., Ellis, R. S., & Sharples, R. M. 1998, ApJ, 497, 188

Couch, W. J., Balogh, M. L., Bower, R. G., et al. 2001, ApJ, 549, 820

Czoske, O., Kneib, J.-P., Soucail, G., et al. 2001, A&A, 372, 391 (CKS)

Czoske, O., Moore, B., Kneib, J. P., & Soucail, G. 2002, A&A, 386, 31

Delaney, M., & Ott, S. 2002, ISOCAM Interactive Analysis User's Manual, Version 5.1, SAI/96-5226/Dc

Dressler, A., Gunn, J. E., & Schneider, D. P. 1985, ApJ, 294, 70

Dressler, A., & Shectman, S. A. 1988, AJ, 95, 985

Dressler, A., & Gunn, J. E. 1992, ApJS, 78, 1 (DG)

Dressler, A., Smail, I., Poggianti, B., et al. 1999, ApJS, 122, 51

Duc, P. A., Poggianti, B., Fadda, D., et al. 2002, A&A, 382, 60

Duc, P. A., Fadda, D., Poggianti, B., et al. 2004 [arXiv:astro-ph/0404183]

Dwarakanath, K. S., & Owen, F. N. 1999, AJ, 118, 625

Elbaz, D., Cesarsky, C., Chanial, P., et al. 2002, A&A, 384, 848

Elbaz, D., & Cesarsky, C. J. 2003, Science, 300, 270

Ellingson, E., Lin, H., Yee, H. K. C., & Carlberg, R. G. 2001, ApJ, 547, 609

Fadda, D., Elbaz, D., Duc, P.-A., et al. 2000, A&A, 361, 827

Franceschini, A., Aussel, H., Cesarsky, C. J., Elbaz, D., & Fadda, D. 2001, A&A, 378, 1

Francis, P. J., Wilson, G. M., & Woodgate, B. E. 2001, PASA, 18, 64

Fujita, Y. 1998, ApJ, 509, 587

Gavazzi, G., & Jaffe, W. 1987, A&A, 186, L1

Genzel, R., & Cesarsky, C. J. 2000, ARA&A, 38, 761

Ghigna, S., Moore, B., Governato, F., et al. 1998, MNRAS, 300, 146

Girardi, M., Fadda, D., Escalera, E., et al. 1997, ApJ, 490, 56

Girardi, M., & Mezzetti, M. 2001, ApJ, 548, 79

Granato, G. L., Silva, L., Monaco, P., et al. 2001, MNRAS, 324, 757

Gruppioni, C., Lari, C., Pozzi, F., et al. 2002, MNRAS, 335, 831

Gunn, J. E., & Gott, J. R. 1972, ApJ, 176, 1

Gunn, J. E., & Oke, J. B. 1975, ApJ, 195, 255

Humason, M. L., & Sandage, A. R. 1957, in Carnegie YearBook 1956 (Carnegie Institute of Washington), 61

Hwang, C., Lo, K. Y., Gao, Y., Gruendl, R. A., & Lu, N. Y. 1999, ApJ, 511, L17

Icke, V. 1985, A&A, 144, 115

Ishida, C. M., & Sanders, D. B. 2001, AAS, 198, 34.16

Jansen, R. A., Fabricant, D., Franx, M., & Caldwell, N. 2000, ApJS, 126, 331

Kassiola, A., Kovner, I., Fort, B., & Mellier, Y. 1994, ApJ, 429, L9

Kauffmann, G., & Haehnelt, M. 2000, MNRAS, 311, 576

Kennicutt, R. C. 1992, ApJ, 388, 310

Kennicutt, R. C. 1998, ARA&A, 36, 189

Kessler, M., Steinz, J., Anderegg, M., et al. 1996, A&A, 315, L27

King, L. J., Clowe, D. I., & Schneider, P. 2002, A&A, 383, 118

Kneib, J.-P., Hudelot, P., Ellis, R. S., et al. 2003, ApJ, 598, 804K

Kodama, T., Balogh, M., Smail, I., Bower, R., & Nakata, F. MNRAS, in press [arXiv:astro-ph/0408037]

Koo, D. 1988, in Large-Scale Motions in the Universe, ed. V. G. Rubin, & G. V. Cayne (Princeton Univ. Press), p. 513

Lari, C., Pozzi, F., Gruppioni, C., et al. 2001, MNRAS, 325, 1173
Laurent, O., Mirabel, I., Charmandaris, V., et al. 2000, A&A, 359, 887
Lavery, R. J., & Henry, J. P. 1986, ApJ, 304, L5
Leech, K. J., Völk, H. J., Heinrichsen, I., et al. 1999, MNRAS, 310, 317
Lémonon, L., Pierre, M., Cesarsky, C. J., et al. 1998, A&A, 334, L21
Lewis, I., Balogh, M., De Propris, R., et al. 2002, MNRAS, 334, 673
López-Sánchez, Á. R., Esteban, C., & Rodríguez, M. 2004, ApJS, 153, 243
Madau, P., Ferguson, H. C., Dickinson, M. E., et al. 1996, MNRAS, 283, 1388
Mann, R. G., Oliver, S., Carballo, R., et al. 2002, MNRAS, 332, 549
McCracken, H. J., Radovich, M., Bertin, E., et al. 2003, A&A, 410, 17
McLean, I. S., & Teplitz, H. 1996, AJ, 112, 2500 (MT)
Mellier, Y., Fort, B., Soucail, G., Mathez, G., & Cailloux, M. 1991, ApJ, 380, 334
Mercurio, A., Girardi, M., Boschin, W., Merluzzi, P., & Busarello, G. 2003, A&A, 397, 431
Metcalfe, L., McBreen, B., Kneib, J. P., & Altieri, B. 2001, IAU Symp., 204, 217
Metcalfe, L., Kneib, J. P., McBreen, B., et al. 2003, A&A, 407, 791
Mihos, J. C. 2004, Carnegie Observatories Astrophysics Series, Vol. 3 (Cambridge: Cambridge Univ. Press), 278
Miville-Deschênes, M.-A., Boulanger, F., Abergel, A., & Bernard, J.-P. 2000 A&AS, 146, 519
Moore, B., Katz, N., Lake, G., Dressler, A., & Oemler, A. 1996, Nature, 379, 613
Morris, S. L., Hutchings, J. B., Carlberg, R. G., et al. 1998, ApJ, 507, 84
Moss, C., & Whittle, M. 1997, Rev. Mex. Astron. Astrof. Conf. Ser., 6, 145
Navarro, J. F., Frenk, C. S., & White, S. 1997, ApJ, 490, 493
Oemler, A. J., Dressler, A., & Butcher, H. R. 1997, ApJ, 474, 561
Okumura, K. 1998, ESA ISOCAM PSF report `http://iso.vilspa.esa.es/users/expl_lib/CAM/psf_report.ps.gz`
Oliver, S., Rowan-Robinson, M., Alexander, D. M., et al. 2000, MNRAS, 316, 749
Ota, N., Hattori, M., Pointecouteau, E., & Mitsuda, K. 2004, ApJ, 601, 120
Ott, S., Abergel, A., Altieri, B., et al. 1997, in Astronomical Data Analysis Software and Systems (ADASS) VI, ed. G. Hunt, & H. E. Payne (San Francisco: ASP), ASP Conf. Ser., 125, 34
Pickles, A. J., & van der Kruit, P. C. 1991, A&AS, 91, 1 (P)
Pierre, M., Aussel, H., Altieri, B., et al. 1996, A&A, 315, L297
Poggianti, B. M., Smail, I., Dressler, A., et al. 1999, ApJ, 518, 576
Schuecker, P., Böhringer, H., Reiprich, T. H., & Feretti, L. 2001, A&A, 378, 408
Quillen, A. C., Rieke, G. H., Rieke, M. J., Caldwell, N., & Engelbracht, C. W. 1999, ApJ, 518, 632
Rakos, K. D., & Schombert, J. M. 1995, ApJ, 439, 47
Ramirez, A. C., & de Souza, R. E. 1998, ApJ, 496, 693
Rengarajan, T. N., Karnik, A. D., & Iyengar, K. V. K. 1997, MNRAS, 290, 1
Rowan-Robinson, M. 2003, MNRAS, 345, 819
Sanders, D. B., & Mirabel, I. F. 1996, ARA&A, 34, 749
Sato, Y., Kawara, K., Cowie, L. L., et al. 2003, A&A, 405, 833
Schmidt, M., Schneider, D. P., & Gunn, J. E. 1986, ApJ, 306, 411
Schneider, D., Dressler, A., & Gunn, J. 1986, AJ, 92, 523 (SDG)
Serjeant, S., Oliver, S., Rowan-Robinson, M., et al. 2000, MNRAS, 316, 768
Silva, L., Granato, G. L., Bressan, A., & Danese, L. 1998, ApJ, 509, 103
Smail, I., Ellis, R. S., Aragon-Salamanca, A., et al. 1993, MNRAS, 263, 628
Smail, I., Dressler, A., Couch, W. J., et al. 1997, ApJS, 110, 213 (SDC)
Smail, I., Morrison, G., Gray, M. E., et al. 1999, ApJ, 525, 609
Soucail, G., Ota, N., Böhringer, H., et al. 2000, A&A, 355, 433 (S)
Stanford, S. A., Eisenhardt, P. R., & Dickinson, M. 1998, ApJ, 492, 461
Steidel, C. C., Adelberger, K. L., Giavalisco, M., Dickinson, M., & Pettini, M. 1999, ApJ, 519, 1
Treu, T., Ellis, R. S., Kneib, J., et al. 2003, ApJ, 598, 804
Tuffs, R. J., Popescu, C. C., Pierini, D., et al. 2002a, ApJS, 139, 37
Tuffs, R. J., Popescu, C. C., Pierini, D., et al. 2002b, ApJS, 140, 609
Tyson, J. A., Kochanski, G. P., & dell'Antonio, I. P. 1998, ApJ, 498, L107
van Dokkum, P. G., Franx, M., Kelson, D. D., et al. 1998, ApJ, 500, 714
Veilleux, S., Kim, D.-C., & Sanders, D. B. 2002, ApJS, 143, 315
Wallington, S., Kochanek, C., & Koo, D. C. 1995, ApJ, 441, 58
Werner, M. W., Roellig, T. L., Low, F. J., et al. 2004, ApJS (Spitzer Special Issue), accepted
Zhang, Y.-Y., Böhringer, H., Mellier, Y., Soucail, G., & Forman, W. 2005, A&A, 429, 85